



This is a repository copy of *Reaction mechanisms and kinetics in geopolymers incorporating strontium salts*.

White Rose Research Online URL for this paper:

<https://eprints.whiterose.ac.uk/id/eprint/229127/>

Version: Published Version

Article:

O'Donoghue, K.T., Geddes, D., Hayes, M. et al. (1 more author) (2025) Reaction mechanisms and kinetics in geopolymers incorporating strontium salts. *Dalton Transactions*, 54 (29). 11337-11348. ISSN: 1477-9226

<https://doi.org/10.1039/d5dt01087j>

Reuse

This article is distributed under the terms of the Creative Commons Attribution (CC BY) licence. This licence allows you to distribute, remix, tweak, and build upon the work, even commercially, as long as you credit the authors for the original work. More information and the full terms of the licence here:

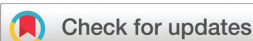
<https://creativecommons.org/licenses/>

Takedown

If you consider content in White Rose Research Online to be in breach of UK law, please notify us by emailing eprints@whiterose.ac.uk including the URL of the record and the reason for the withdrawal request.



eprints@whiterose.ac.uk
<https://eprints.whiterose.ac.uk/>



Cite this: DOI: 10.1039/d5dt01087j

Reaction mechanisms and kinetics in geopolymers incorporating strontium salts

Kyle T. O'Donoghue,^a Daniel A. Geddes,^a Martin Hayes^b and Brant Walkley *^a

Geopolymers are promising materials for immobilisation of ⁹⁰Sr, present in complex radioactive waste streams at sites such as Sellafield and Fukushima Daiichi. This study investigates the impact of strontium salts (Sr(OH)₂·8H₂O, SrCO₃, Sr(NO₃)₂, and SrSO₄) on geopolymer reaction mechanisms and kinetics. Isothermal conduction calorimetry, zeta potential, and X-ray diffraction data show that the introduction of the strontium salt leads to a reduction in the rate and extent of reaction. This is a result of (1) reduced dissolution of the metakaolin precursor due to (a) a reduction in pH of the aqueous phase and (b) sorption of Sr²⁺ cations to the surface of the metakaolin precursor, and (2) a 'filler effect' arising from the presence of insoluble solid particles of the strontium salts. The extent to which each mechanism occurs depends on the salt solubility in the high pH, high ionic strength fresh cement slurry. This insight is vital for designing geopolymer cements for the long-term immobilisation of radioactive waste streams containing ⁹⁰Sr.

Received 8th May 2025,
Accepted 30th June 2025
DOI: 10.1039/d5dt01087j

rsc.li/dalton

1. Introduction

Electricity generation *via* nuclear fission in the civil sector produces an array of radioactive waste streams which must be conditioned and safely disposed of to prevent release to the surrounding environment. An example of such waste is strontium-90 (⁹⁰Sr), which forms as a fission product and can be found in complex legacy nuclear waste streams at sites such as Sellafield and Fukushima Daiichi nuclear power plants. The safe containment of ⁹⁰Sr is of international importance as many countries explore and prioritise development of deep geological disposal facilities (GDF) for disposal of radioactive waste.¹ The selection of the encapsulating material that provides the initial engineered barrier of containment plays a crucial role in this.

Cementation has recently been explored as a promising low cost, low temperature technology for the conditioning of radioactive wastes containing ⁹⁰Sr.^{2–4} The presence of ⁹⁰Sr in aqueous waste streams often necessitates its extraction using granular inorganic ion exchange materials, making cementation a very suitable conditioning route for this type of waste. Furthermore, ⁹⁰Sr exhibits a relatively short half-life (*t*_{1/2} = 28.80 years), which means that ⁹⁰Sr-bearing cement waste-forms are only required to be durable and secure for a few hundred years.

Traditionally, portland cement (PC) has been investigated for encapsulation of ⁹⁰Sr-bearing wastes, and has been shown to be capable of binding Sr through chemisorption to the calcium silicate hydrate (C–S–H) gel phase. The substitution of Ca²⁺ ions by ⁹⁰Sr²⁺ ions within the hydrate phases of PC, most notably C–S–H, has also been observed.^{2,5} However, much of the ⁹⁰Sr uptake comes in the form of reversible ion exchange reactions to hydrated and partially hydrated phases within hardened PC.⁵ This limits the potential degree of chemical immobilisation, leading to much of the Sr waste being simply physically encapsulated (rather than chemically bound) within the cement binder. Furthermore, the high water content of hydrated PC can detrimentally affect the radiolytic stability of the wasteform.⁶ The high CO₂ emissions associated with the production of PC – 8% of anthropological CO₂ emissions globally – is a further issue which is becoming more prominent in the current climate, and is viewed as increasingly important in the nuclear sector.^{7,8} Therefore, research into alternative cementitious materials is vital to develop a sustainable, high-performance material for the safe and effective containment of ⁹⁰Sr-bearing wastes.

More recently, geopolymers, an alkali-activated aluminosilicate cement binder, have been considered as a promising alternative to Portland cement-based encapsulants. Geopolymers comprise a structurally disordered, highly cross-linked alkali aluminosilicate gel framework containing cation binding sites which possess the potential to incorporate cations, such as Sr²⁺, into the gel framework *via* ion exchange.^{9–11} This, as well as their desirable chemical, mechanical and thermal properties, has led to a significant

^aSchool of Chemical, Materials and Biological Engineering, The University of Sheffield, Sheffield S1 3JD, UK. E-mail: b.walkley@sheffield.ac.uk

^bUnited Kingdom National Nuclear Laboratory, Warrington, UK



level of interest surrounding geopolymers as a matrix for the immobilisation and subsequent disposal of radioactive waste.^{11–13}

The most common alkali metals used to produce geopolymers are sodium and potassium, leading to the primary alkali aluminosilicate hydrate gel network being abbreviated to (N, K)-A-S-H (sodium or potassium aluminosilicate hydrate). The nanostructure is described as pseudo-zeolitic; it is identical to that of a zeolite over short distances (no greater than several angstrom),^{14,15} yet over longer distances the alkali aluminosilicate gel exhibits extensive disorder, and is completely X-ray amorphous, contrasting with crystalline zeolites. Similar to zeolites, geopolymers comprise Si and Al in tetrahedral coordination, with the chemical environment of Si being described using $Q^n(mAl)$ nomenclature (where n is the number of other bonded tetrahedral units *via* oxygen bridges, of which m is the number of these units that are Al tetrahedra), most commonly $Q^4(mAl)$ and Al existing most commonly in the $q^4(4Si)$ coordination. The negative charge that arises from Al^{3+} in four-fold coordination is charge-balanced by the presence of alkali metal cations in extra-framework sites.

Previous work has focused primarily on the interaction between sodium silicate-activated geopolymers and strontium containing waste simulants, yet within the context of encapsulation of radioactive waste within the nuclear sector potassium silicate-activated geopolymers have been shown to exhibit more preferential flow characteristics and rheological properties than equivalent sodium activated geopolymer formulations.^{16–18} This is particularly important in the context of cementation of radioactive waste streams exhibiting complex shapes and morphologies, where a fluid fresh-state paste is essential for sufficient encapsulation.

The kinetics of reaction of the soluble alkali and silica constituents and the solid aluminosilicate precursor (typically metakaolin), and subsequent alkali aluminosilicate gel formation, dictate the initial setting period of the geopolymer.^{19,20} An understanding of these properties allows for the initial phase of reaction to be tailored to its application; for example, altering the rate of reaction to extend the period of desirable workability, and to maintain fluidity which allows for better infill of complex waste types with tortuous pathways, producing a lower porosity wasteform. The order in which the components of the geopolymer reaction mixture are added together can also significantly alter the early stage kinetics of reaction; there are varying observations in the literature about the rate at which the reaction occurs, and an understanding of the role of each constituent and its point of addition carries both scientific and industrial importance.

This work investigates the impact of incorporating various salts of non-radioactive isotopes of strontium (Sr) on the kinetics and mechanisms of the reaction within the fresh cement paste, and early stage K-A-S-H gel formation of potassium silicate-activated geopolymers. The chemical environments created by the introduction of $Sr(OH)_2 \cdot 8H_2O$, $SrCO_3$, $Sr(NO_3)_2$ and $SrSO_4$ to the geopolymer reaction mixture simulate the potential interactions observed when

complex waste streams resulting from *e.g.* cooling water, radioactive sludge/slurries, spent-ion exchange materials, *etc.*, containing Sr are encapsulated/immobilised within a geopolymer wasteform.

Isothermal conduction calorimetry (ICC) is used to monitor the heat evolution during reaction, and zeta potential measurements are taken to determine the electrokinetic potential on the surface of the solid reactant particles, which can help to reveal the reaction mechanisms occurring. X-ray diffraction (XRD) is used to reveal any crystalline reaction products present within the geopolymers. The findings of this work provide an important overview of the early stage reactions within the geopolymer wasteforms, and how these are influenced by various salts of non-radioactive isotopes of strontium (Sr). This reveals the distinct mechanisms driving the initial dissolution of metakaolin and subsequent K-A-S-H gel formation, and suggests that geopolymers are suitable for the long-term immobilisation of radioactive waste streams containing ⁹⁰Sr.

2. Materials and methods

2.1 Geopolymer sample production

2.1.1 Geopolymer cements. The geopolymers in this study were produced by the reaction of MetaMax metakaolin (MK) (BASF) with a potassium silicate activating solution. The chemical composition of the metakaolin, as obtained by X-ray Fluorescence (XRF), can be found in Table 1. The activating solution was made by reacting potassium hydroxide (AnalaR 99 wt%), deionised water and a potassium silicate solution (PQ-KS, 51.6% potassium silicate, with a solution modulus of SiO_2/K_2O of 2.2, with the balance water, PQ-UK).

Stoichiometry was designed to obtain an activating solution modulus $SiO_2/K_2O = 1$, an activator dose such that $K_2O/Al_2O_3 = 1$, and a water content molar ratio of $H_2O/K_2O = 11$.

The amount of strontium hydroxide octahydrate ($Sr(OH)_2 \cdot 8H_2O$) (Acros Organics, 98%), strontium carbonate ($SrCO_3$) (Sigma Aldrich, >99.9%), strontium nitrate ($Sr(NO_3)_2$) (Alfa Aesar, 98%) and strontium sulphate ($SrSO_4$) (Alfa Aesar, Reagent Grade) added to the samples was determined by setting a constant Sr/Al molar ratio in the final geopolymer binder, as shown by Table 2.

To produce the geopolymers containing the Sr salts, the salt is mixed with the metakaolin powder before the introduction of the activating solution. The resulting mixture is mixed

Table 1 Chemical composition (wt%) of the MetaMax metakaolin used in this work, obtained by X-ray fluorescence (XRF)

SiO ₂	Al ₂ O ₃	TiO ₂	Fe ₂ O ₃	CaO	Na ₂ O	Others	Loss on Ignition (1000 °C)
52.54	44.54	1.31	0.36	Trace	0.15	0.20	0.63



Table 2 The geopolymer formulations used in this work, with and without Sr salts, with the corresponding anion and nominal Sr/Al, Si/Al, K/Al, H₂O/K₂O and w/s molar ratios

Sample	Anion	Sr/Al ratio	Si/Al ratio	K/Al ratio	H ₂ O/K ₂ O ratio	w/s ratio
KGP	—	—	1.5	1.0	11	0.55
OH_1	OH ⁻	0.025	1.5	1.0	11	0.55
OH_2	OH ⁻	0.050	1.5	1.0	11	0.55
OH_3	OH ⁻	0.075	1.5	1.0	11	0.54
OH_5	OH ⁻	0.125	1.5	1.0	11	0.54
CO ₃ _1	CO ₃ ²⁻	0.025	1.5	1.0	11	0.56
CO ₃ _2	CO ₃ ²⁻	0.050	1.5	1.0	11	0.57
CO ₃ _3	CO ₃ ²⁻	0.075	1.5	1.0	11	0.58
CO ₃ _5	CO ₃ ²⁻	0.125	1.5	1.0	11	0.60
NO ₃ _1	NO ₃ ⁻	0.025	1.5	1.0	11	0.56
NO ₃ _2	NO ₃ ⁻	0.050	1.5	1.0	11	0.58
NO ₃ _3	NO ₃ ⁻	0.075	1.5	1.0	11	0.59
NO ₃ _5	NO ₃ ⁻	0.125	1.5	1.0	11	0.62
SO ₄ _1	SO ₄ ²⁻	0.025	1.5	1.0	11	0.56
SO ₄ _2	SO ₄ ²⁻	0.050	1.5	1.0	11	0.57
SO ₄ _3	SO ₄ ²⁻	0.075	1.5	1.0	11	0.57
SO ₄ _5	SO ₄ ²⁻	0.125	1.5	1.0	11	0.60

for 10 minutes before being stored in a sealed container at 20 °C. At the desired curing times (3 and 28 days' post-reaction), a section of each geopolymer sample was removed from storage before being immersed in isopropanol to halt the alkali-activation reaction through the removal of loosely bound water. For this work, one batch of each sample was prepared; as a result all of the analysis techniques are carried out on samples from the same batch.

2.2 Sample characterisation

2.2.1 Isothermal conduction calorimetry. Isothermal conduction calorimetry was used to examine the heat evolution during the reaction and, therefore, study the kinetics of the reaction between the activating solution and the metakaolin powder.²¹ Heat evolution in the geopolymer pastes was measured at 20 °C for a total of 7 days using dual channel TAM Air Isothermal Conduction Calorimeter from TA instruments. 20 g of each geopolymer was mixed within the glass ampoule using a vortex mixer to provide uniform mixing for two minutes before insertion into the calorimeter.

2.2.2 Zeta potential. Zeta potential measurements were performed to determine the electrokinetic potential on the surface of the metakaolin particles in solution. 20 g samples were used, each containing 2 g of metakaolin and the corresponding mass of the salt required to reach the Sr/Al ratios used in the entirety of this work, in a solution of potassium hydroxide (KOH) at pH 10 and pH 12. The zeta potential of the dispersions was measured using a Stabino II system from Colloid Metrix. The samples were mixed *via* 10 inversions, and the readings were taken 30 seconds after the initial mixing. Error bars in the data show the standard deviation of 3 rounds of data collection.

2.2.3 X-ray diffraction. X-ray diffraction (XRD) data were obtained to examine the long range ordering and crystallinity of the reaction products in each sample, using the same method as in previous work.²² Data were obtained using a Panalytical X'Pert³ Powder X-ray diffractometer across a 2θ range of 5°–70°, with Cu K α radiation (1.54 Å), a nickel filter, a step size of 0.020°, and a count time of 1 s per step. Low angle diffracted background intensity was reduced using an anti-scatter blade. An incident beam divergence of 1.0 mm and a 2.5° Soller slit in the diffracted beam were used.

3. Results and discussion

3.1 Geopolymers incorporating Sr(OH)₂·8H₂O

3.1.1 Isothermal conduction calorimetry. Fig. 1(a) displays the isothermal calorimetry curves obtained when measuring heat evolution during the reaction of the K-geopolymers loaded with Sr(OH)₂·8H₂O over the first 3 days of reaction. Each of the curves display a single, complete, broad peak within the first 2 days of reaction. Previous work shows that the reaction process for geopolymers produces three distinct peaks in the calorimetry data;²³ in that work, dissolution of the metakaolin as a result of the high pH of the activating solution is attributed to the appearance of an initial peak, which usually occurs within the first few minutes of reaction. The method used in the current work presented here does not allow for this peak to be fully observed in its full state due to the initial mixing of the reaction mixture occurring outside of the calorimeter. Therefore, any sign of this first peak will be disregarded and all observations will be taken from the second peak, which is attributed to the heat produced from the formation of the aluminosilicate framework as observed in Fig. 1.

Fig. 1(a) shows that the addition of Sr(OH)₂·8H₂O has a mild retarding effect on the kinetics of the reaction process when compared to the KGP control sample. Increasing the Sr/Al ratio increases the level of retardation of the reaction, as the maximum observed heat flow both decreases, and occurs later in the reaction. The solubility of Sr(OH)₂·8H₂O is very low, and is not expected to fully dissolve into solution when combined with the activator.²⁴ Therefore, the effect of the addition of the salt on the kinetics will be partially due to a portion of the salt acting as an inert filler material within the binder. However, the presence of an inert material (the filler effect) alone does not account for the magnitude of reduction in heat flow during the reaction observed in Fig. 1(a).

Fig. 2(a) shows that the relationships between Sr/Al ratio and both time and value of the maximum heat evolution of the visible peak in the data are approximately linear, although the effect begins to dampen between an Sr/Al ratio of 0.075 and 0.125. This suggests that the maximum retardation of reaction caused by Sr(OH)₂·8H₂O within this KGP formulation is reached around this region, as adding more of the salt above an Sr/Al ratio of 0.075 has less of an effect on the kinetics of reaction when compared to the salt addition at a lower Sr/Al ratio. However, the reduction in heat does not reduce to



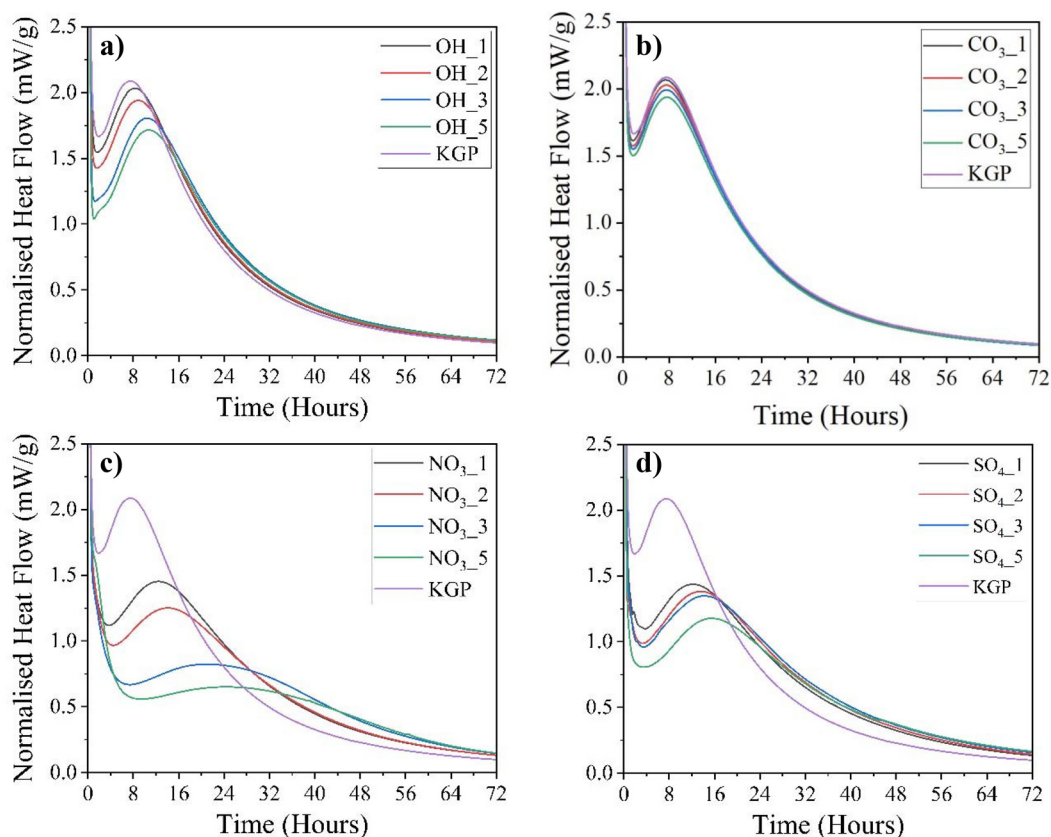


Fig. 1 Calorimetry curves for the geopolymers showing normalised heat flow (mW per g of sample) over the first 3 days of reaction. Plot (a) shows the geopolymers loaded with $\text{Sr}(\text{OH})_2 \cdot 8\text{H}_2\text{O}$, plot (b) the geopolymers loaded with SrCO_3 , plot (c) the gels loaded with $\text{Sr}(\text{NO}_3)_2$ and plot (d) the geopolymers loaded with SrSO_4 .

0, as adding the salt continues to add to the filler effect. The pattern seen in Fig. 1 is followed in Fig. 3(a), as the cumulative heat release, and therefore reaction completion percentage, decreases with increasing Sr/Al ratio.

3.1.2 Zeta potential measurements. The interactions of the Sr^{2+} cations with the solid metakaolin particles and aqueous phase in the fresh geopolymer paste can be partially explained by the zeta potential values of dispersions of metakaolin particles in solution with varying Sr/Al ratios, as shown in Fig. 4.

The zeta potential values for the metakaolin dispersions with an Sr/Al ratio of 0, become less negative as the pH increases from pH 10 to pH 12. This could suggest that the electrostatic repulsion between the metakaolin particles decreases within this pH change, leading to a lesser rate of dissolution of the metakaolin. However, it is more likely that the increased pH of the system leads to a higher rate of dissolution of the metakaolin, which in turn decreases the magnitude of the observed zeta potential values. This has been reported in previous work, where Derkani *et al.* showed that the dissolution of metakaolin occurs at a higher rate at a higher pH.²⁸

Derkani *et al.* describe the effect of K^+ ions on the surface charge of metakaolin, showing that the inclusion of these ions in the solution leads to a change in the recorded zeta potential

value.²⁸ They also show that the further introduction of divalent cations, such as the Sr^{2+} seen in this work, leads to an increase of the recorded zeta potential towards a value of 0.²⁸ This is due to the cation adsorbing to the surface of the metakaolin particles. Therefore, both the Sr^{2+} and the K^+ ions in solution will be impacting the surface charge of the metakaolin.

The zeta potential results here suggest that the solubility of $\text{Sr}(\text{OH})_2 \cdot 8\text{H}_2\text{O}$ is not affected by the pH of the solution, as the zeta potential trends follow similar trajectories between pH 10 and pH 12. There is a slight deviation in the data for Sr/Al ratios of 0.05 and 0.075, but the overall trend is comparable. At a Sr/Al ratio of 0.125, the recorded zeta potential reaches a maximum value of around -12.4 mV. This is due to the positively charged Sr^{2+} ions adsorbing to the surface of the metakaolin. It can be assumed that this would also be similar in the geopolymer systems themselves at the much higher pH seen in the real systems.

The presence of K^+ cations from the KOH solution will lead to a shift in the zeta potential towards more positive values, as these cations will also adsorb to negative sites on the metakaolin surface, caused by the deprotonation of the surface hydroxyl sites in the alkaline solution, as well as AlO_4 sites in the geopolymer gel, leading to an increased negative charge on



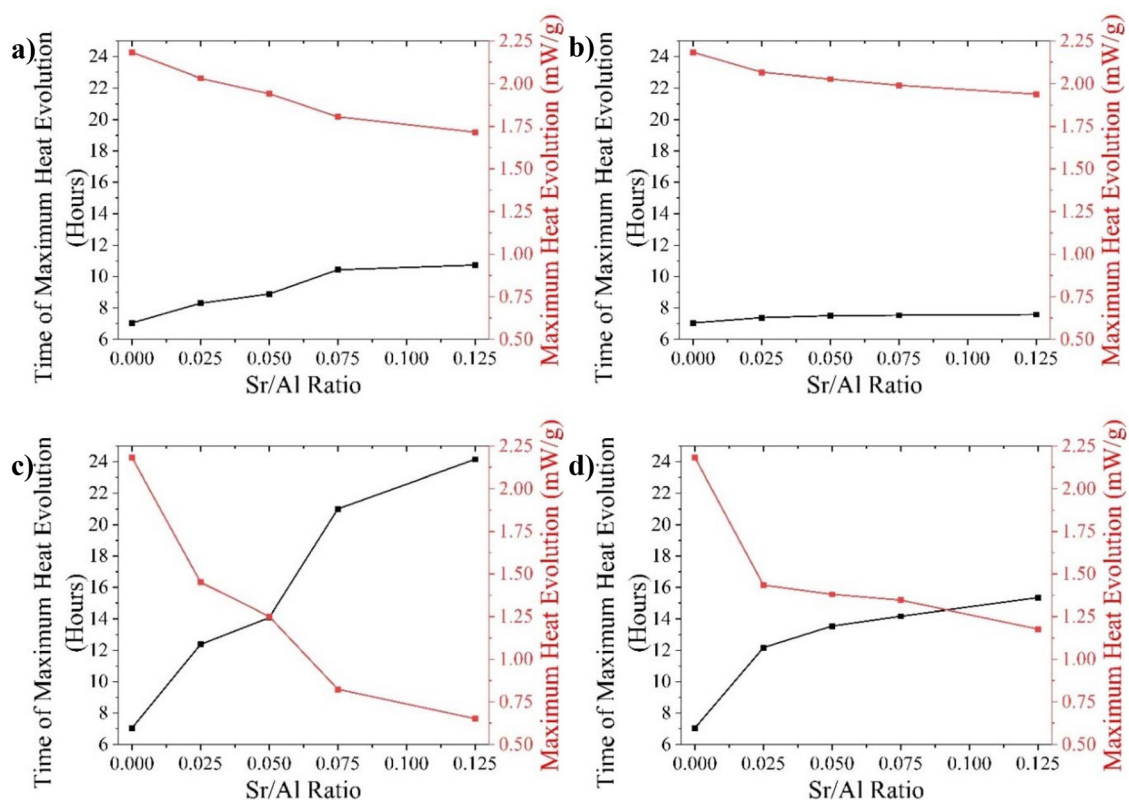


Fig. 2 The relationship between Sr/Al ratio and the observed time of maximum heat evolution and the value of the maximum heat evolution. Plot (a) shows the geopolymers loaded with Sr(OH)₂·8H₂O, plot (b) the geopolymers loaded with SrCO₃, plot (c) the geopolymers loaded with Sr(NO₃)₂ and plot (d) the gels loaded with SrSO₄.

the surface of the particles.²⁸ However, the concentration of K⁺ ions is not altered when the Sr/Al ratios are varied at both pH values investigated here. Therefore, there will be the same number of K⁺ cations when the zeta potential is at −97.7 mV (pH 10, Sr/Al ratio of 0) as when the zeta potential is −12.4 mV (pH 10, Sr/Al ratio of 0.125). Therefore, due to the difference in recorded values of zeta potential, it is clear that the main contributor to this change is the introduction of the Sr²⁺ cation. It is also likely that the Sr²⁺ interactions are dominating when compared to the OH[−] ions as the introduction of the OH[−] ions *via* addition of Sr(OH)₂·8H₂O is negligible when compared to the concentration of OH[−] ions already present in solution.

There are two possible mechanisms for the simultaneous observation of decreased heat evolution in the ICC data with increasing Sr/Al ratio, and an increase in zeta potential values with increasing Sr/Al ratio. The first is that the shift in surface charge towards neutral reduces the electrostatic repulsion and therefore dispersion of the metakaolin particles in solution,^{29,30} and promotes their agglomeration. This agglomeration results in a reduction to the total surface area of metakaolin available to participate in reaction during dissolution and, therefore, a reduction in the rate of dissolution of metakaolin. The second is the formation of a layer of Sr²⁺ ions on the surface of the metakaolin particles, producing a physico-chemical barrier that simultaneously lowers the concentration

gradient between the metakaolin and the surrounding solution and shields the surface of the aluminosilicate solid from OH[−] ions in solution, which as a consequence are prevented from breaking the interlayer and intralayer bonds in metakaolin and preventing dissolution. This mechanism has been shown to govern the dissolution of glass, as outlined in Frugier *et al.*,³¹ and as metakaolin is a crystallographically disordered aluminosilicate solid, the concept of a physical barrier to dissolution fits the observations here, as the Sr²⁺ ions are drawn to the surface of the metakaolin. It is likely that it is a combination of both mechanisms that leads to the reduced rate of metakaolin dissolution observed for the geopolymer samples with addition of Sr(OH)₂·8H₂O (*i.e.* containing the OH[−] anion).

The zeta potential values seen in Fig. 4 indicate that the delay in reaction seen in the ICC data are, in some part, due to the effect of the Sr²⁺ cations on the dissolution of the metakaolin. The reduced rate of dissolution leads to a lower concentration of silicon and aluminium particles within the solution, meaning that the reaction to form the alkali aluminosilicate gel cannot occur until a later stage in the reaction process. This effect increases with increasing Sr/Al ratio. The effects on the surface charge of the metakaolin described above, coupled with the presence of relatively inert undissolved Sr(OH)₂·8H₂O that are unable to dissolve due to saturation of Sr in solution



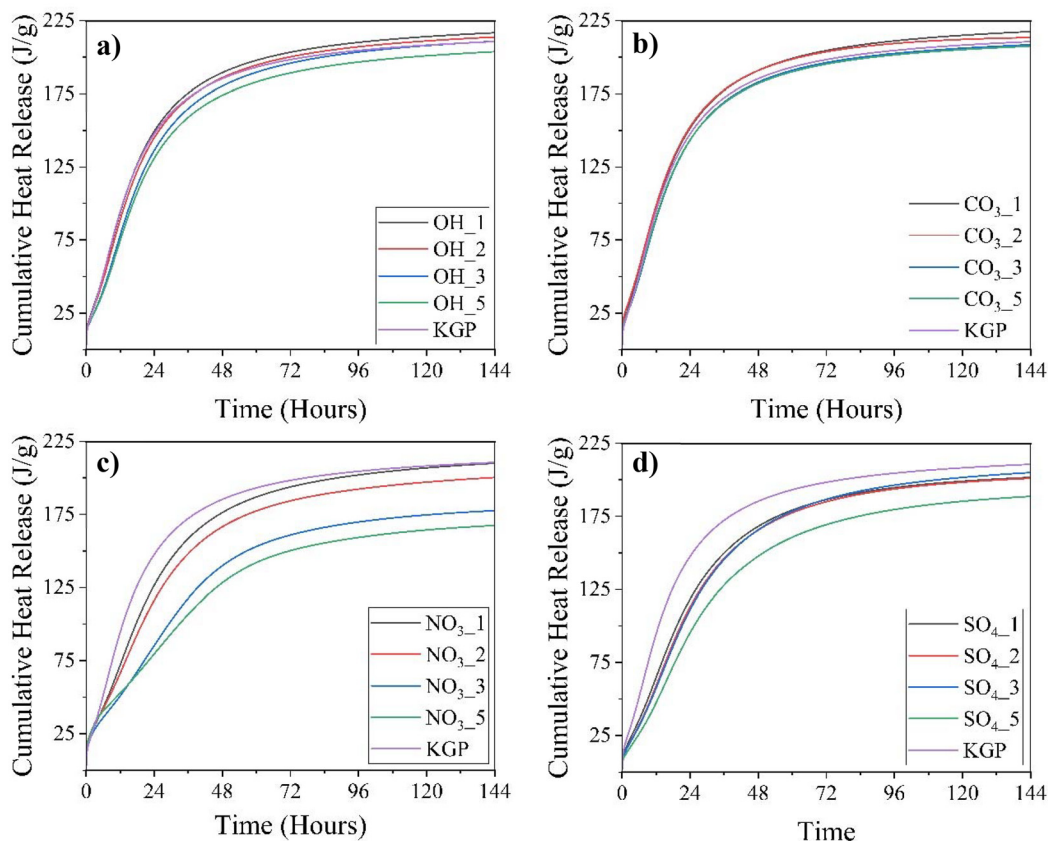


Fig. 3 The cumulative heat release curves over the first 144 hours of reaction. Plot (a) shows the geopolymers loaded with $\text{Sr}(\text{OH})_2 \cdot 8\text{H}_2\text{O}$, plot (b) the geopolymers loaded with SrCO_3 , plot (c) the geopolymers loaded with $\text{Sr}(\text{NO}_3)_2$ and plot (d) the geopolymers loaded with SrSO_4 .

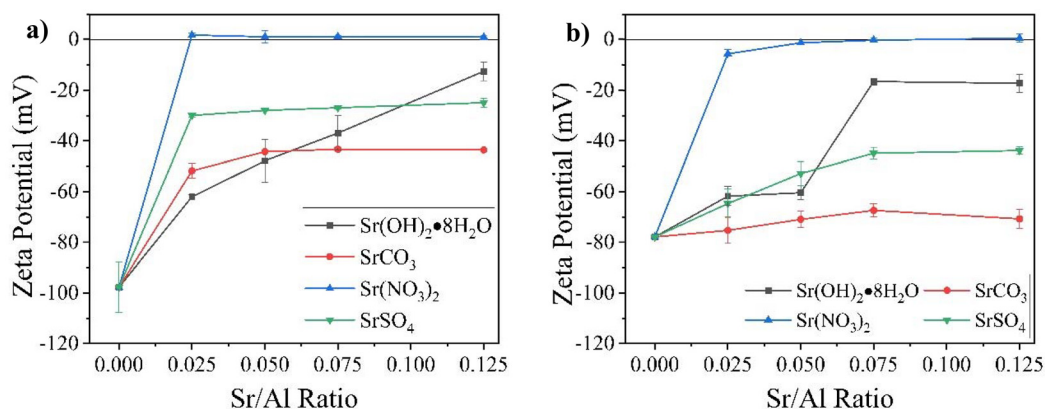


Fig. 4 Comparing the effect of Sr/Al ratio, altered by the addition of $\text{Sr}(\text{OH})_2 \cdot 8\text{H}_2\text{O}$, SrCO_3 , $\text{Sr}(\text{NO}_3)_2$ and SrSO_4 , on the zeta potential of metakaolin particles in a KOH solution at (a) pH 10 and (b) pH 12.

(i.e. the filler effect), leads to the changes to the heat flow observed by ICC during geopolymer reaction.

3.1.3 X-ray diffraction. The XRD data (Fig. 5) for each sample within a set are comparable, exhibiting a broad feature due to diffuse scattering between $24^\circ 2\theta$ and $33^\circ 2\theta$. This peak indicates the presence of an amorphous phase within the sample, and is consistent with the presence of the K-A-S-H gel.³⁴

The XRD data for geopolymers incorporating $\text{Sr}(\text{OH})_2 \cdot 8\text{H}_2\text{O}$ show a broad feature due to diffuse scattering, consistent the formation of the K-A-S-H gel, and also exhibit diffraction peaks due the presence of anatase (TiO_2 , Powder Diffraction file (PDF) # 01-084-1286), which arises due to its presence as an impurity in the metakaolin used in this study. Anatase is inert under the



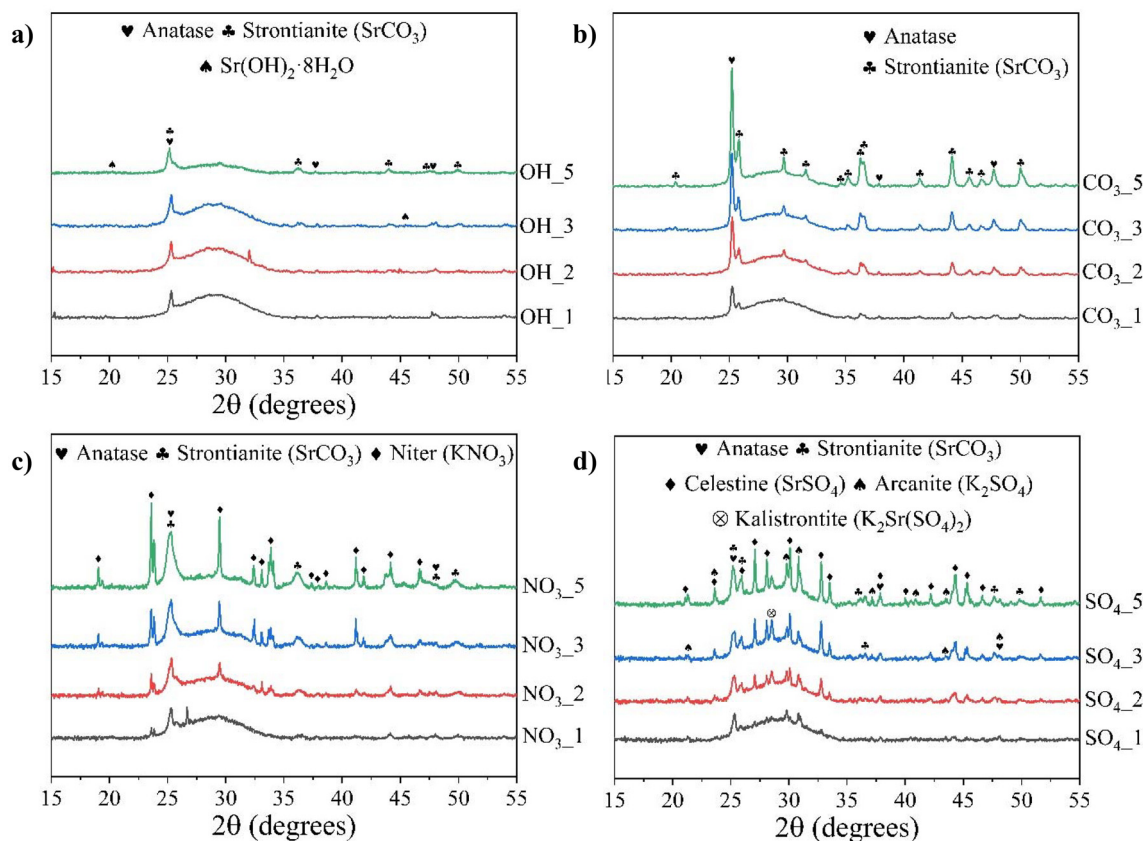


Fig. 5 The X-ray diffraction data of the samples after the first 3 days of reaction. Plot (a) shows the geopolymers loaded with $\text{Sr}(\text{OH})_2 \cdot 8\text{H}_2\text{O}$, plot (b) the gels loaded with SrCO_3 , plot (c) the gels loaded with $\text{Sr}(\text{NO}_3)_2$ and plot (d) the gels loaded with SrSO_4 .

reaction conditions occurring during alkali-activation of metakaolin.

The presence of strontium hydroxide octahydrate ($\text{Sr}(\text{OH})_2 \cdot 8\text{H}_2\text{O}$, PDF # 00-027-1438) in samples OH_3 and OH_5 is expected due to the low solubility of the salt. It is clear that some of the strontium is still in the form in which it was added to the geopolymer mix, and has not dissolved to be incorporated into the structure due to its low solubility. The diffraction peaks for this salt are not present in the spectra for samples OH_1 and OH_2. This could be due to the concentration being too small in the samples as, potentially, a greater percentage of the mass of the salt has dissolved into the activating solution. The diffraction data for the OH_2 sample shows that there is strontianite (SrCO_3 , PDF # 00-005-0418) present. This is most likely due to the carbonation of the geopolymer due to air, forming SrCO_3 crystals.

3.2 Geopolymers incorporating SrCO_3

3.2.1 Isothermal conduction calorimetry. Isothermal conduction calorimetry data in Fig. 1(b) shows that the addition of SrCO_3 to the geopolymers at all Sr/Al ratios has a much lower effect on the heat evolved during reaction. Both the maximum value of normalised heat flow, and the time of maximum heat flow, are only slightly affected by the addition of the salt, however there is a clear correlation of these with

Sr/Al ratio, with the maximum value of normalised heat flow decreasing and the time of maximum heat flow increasing with Sr/Al ratio, albeit by a relatively minimal factor (Fig. 6). To emphasise this, the time of maximum heat evolution for the KGP control sample is approximately 7 hours, almost identical to that of all of the CO_3 containing samples, which have a maximum value of 7.5 hours. The CO_3_5 sample showed the

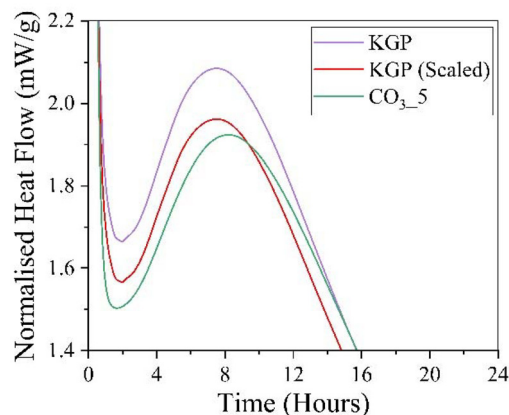


Fig. 6 Calorimetry curves for the KGP and CO_3_5 samples compared to a scaled curve of the KGP sample.



greatest deviation from the control with respect to the maximum recorded heat flow, decreasing by around 11%. This is most likely due to SrCO_3 being an insoluble compound within the fresh geopolymer reaction mixture, and so is unlikely to dissolve within the activating solution. Instead, the solid SrCO_3 particles are suspended within the binder, acting primarily as an inert filling material and slightly retarding the reaction. This is further supported by Fig. 6, which shows the KGP and $\text{CO}_3\text{-5}$ samples seen in this work compared to a scaled version of the curve generated by the KGP sample, shown in red. This is calculated by normalising the heat evolution of the KGP sample by a mass that would be consistent with a $\text{CO}_3\text{-5}$ sample with the same mass of metakaolin and activating solution as the 20 g KGP sample. This curve gives the normalised heat evolution that would be observed if none of the SrCO_3 dissolves into the activating solution, and all SrCO_3 remains as a solid, acting as a filler material in the geopolymer reaction mixture. As can be seen from Fig. 6, the $\text{CO}_3\text{-5}$ sample, shown in green, is not too dissimilar from the scaled KGP curve. This suggests that the majority of the SrCO_3 does not dissolve in the $\text{CO}_3\text{-5}$ sample. However, it is clear that some of the salt does dissolve, exposed by the slight retardation of the reaction when compared to the KGP sample.

Fig. 2(b) shows that as the Sr/Al ratio of the geopolymer mix increases, so does the time at which the maximum heat evolution is reached. However, this effect diminishes as the Sr/Al ratio continues to increase, suggesting that, at some defined point in this region of SrCO_3 addition, the effect of adding more SrCO_3 reaches its maximum. Moreover, the scale of the y-axis should be noted here as the change is on the order of minutes, as opposed to hours. This impact is, in part, due to the addition of the SrCO_3 resulting in a smaller mass of both metakaolin and activating solution available to react and, therefore, produce heat through dissolution. The wt% of the SrCO_3 salt in the $\text{CO}_3\text{-5}$ sample is 6.1%, and the maximum drop in heat flow observed for this sample drops by ~11% compared to the KGP control, suggesting that the decline in available reactive material is likely contributing for the reduction in heat flow. Furthermore, it is likely that ‘wetting’ of the SrCO_3 molecules is occurring, with the activating solution becoming adhered to the surface of the salt, preventing it from commencing the dissolution reaction in the first instance. A combination of these two explanations is the likely cause of the decrease in heat flow, suggesting that no changes are expected to be found in the structure of the resulting geopolymer matrices. Fig. 3(b) follows the same expected pattern, with slight decreases to the cumulative heat as more of the SrCO_3 is loaded into the geopolymer mix, reducing the total mass of reactants within the mix.

3.2.2 Zeta potential measurements. Fig. 4 shows that increasing solution pH has a clear effect on the zeta potential values of the metakaolin particles in the presence of SrCO_3 . As previously mentioned, the addition of the divalent cation Sr^{2+} results in a change in surface charge due to the electrostatic attraction of Sr^{2+} to the negatively charged deprotonated hydroxyl sites on the surface of the metakaolin. The magni-

tude of this change is directly related to both the pH, and the concentration of Sr^{2+} cations within the solution; the increase in the pH from pH 10 to pH 12 leads to a less significant change to the zeta potential with increasing Sr/Al ratio. This correlates with the reduced solubility of SrCO_3 at higher solution pH values, meaning that there are less Sr^{2+} ions available in solution to interact with the surface of the metakaolin.

At pH 10, the introduction of the SrCO_3 causes the zeta potential values to shift towards more positive values, and finally reaching a value of approximately -50 mV. This is likely due to the interactions with the Sr^{2+} cations with the negatively charged deprotonated hydroxyl groups on the surface of the metakaolin. However, this increase, when compared to metakaolin in solution without the presence of Sr, is not affected by the increasing Sr/Al ratio. This is due to the low solubility of SrCO_3 , meaning that only a small amount of the salt dissolves before the solubility limit is reached, and the solution is saturated with the salt at the Sr/Al ratio of 0.025.

However, at pH 12, increasing the Sr/Al ratio does lead to some dissolution of the salt, as the zeta potential values recorded increase towards 0 as the Sr/Al ratio increases. However, this increase is still minimal, as the surface charge of the metakaolin remains very negative. When compared to the pH 10 data, the maximum increase toward 0 is far less; a 10% increase as opposed to a 55% increase. Therefore, it is likely that at the high pH of the geopolymer samples used in this work, around pH 14, the SrCO_3 will not dissolve significantly and will therefore have negligible effect on surface charge of the metakaolin particles. This is supported by the data obtained *via* ICC (Fig. 1b), providing further evidence that the majority of the SrCO_3 does not dissolve into solution and simply acts as a filler within the geopolymer matrix. However, the ICC results do suggest that a small portion of the salt does dissolve, and it is likely that the Sr that is introduced into solution adsorbs onto the surface of the metakaolin to produce the slight increase in zeta potential values seen here. This is comparable to what can be seen with the $\text{Sr}(\text{OH})_2 \cdot 8\text{H}_2\text{O}$ loaded samples, with the inclusion of SrCO_3 into the reaction mixture leading to a change in the rate of reaction through both the filler effect and the interaction of Sr^{2+} ions with the metakaolin.

3.2.3 X-ray diffraction. The XRD data for geopolymers incorporating SrCO_3 show a broad feature due to diffuse scattering, consistent the formation of the K-A-S-H gel, and also exhibit diffraction peaks due to the crystalline strontianite phase (SrCO_3 , PDF # 00-005-0418), indicating that the addition of the SrCO_3 did not lead to its complete dissolution within the activating solution. This is supported by the low solubility limits exhibited by the SrCO_3 , and also by the ICC data (Fig. 1(b)). The presence of anatase (TiO_2 , PDF # 01-084-1286) is also observed, due to its inert nature and presence as an impurity in the metakaolin used in this study.

3.3 Geopolymers incorporating $\text{Sr}(\text{NO}_3)_2$

3.3.1 Isothermal conduction calorimetry. Fig. 1(c) shows that the addition of $\text{Sr}(\text{NO}_3)_2$ to the geopolymer reaction



mixture has an impact on the kinetics of reaction within the first 72 hours. Firstly, the maximum recorded normalised heat flow for the reaction peak decreases with the increasing addition of $\text{Sr}(\text{NO}_3)_2$; the maximum value recorded for the NO_3_5 sample, where the maximum recorded heat flow value is most impacted, is around 30% of the maximum recorded value for the KGP control sample. Furthermore, the time at which the maximum values are recorded is much later in the reaction, with this milestone being reached over 3 times later in the NO_3_5 sample (~26 hours) when compared to the KGP control sample (~7.5 hours). The time period between the initial dissolution peak and the secondary reaction peak (the time in the reaction which would be referred to as the induction period in a PC based system) increases as the Sr/Al ratio increases, further adding to the delay in reaction.

Fig. 2(c) shows that the relationship between the Sr/Al ratio of the geopolymer mix and both the value and time of maximum heat evolution is approximately linear, increasing the time of max heat evolution with increasing Sr/Al ratio and, likewise, decreasing the maximum value of heat evolved with increasing Sr/Al ratio. This also suggests that this trend would continue as the Sr/Al ratio further increases, suggesting that the addition of the salt leads to its subsequent reaction with the raw materials (most probably the activating solution) in a way which either consumes the reactants or prevents the dissolution reaction. This trend suggests that this effect will continue to increase with further addition of the salt.

The results shown here suggest that the addition of the Sr $(\text{NO}_3)_2$ alters the reaction pathways followed within the geopolymer mix during the early phase reaction. $\text{Sr}(\text{NO}_3)_2$ is very soluble, dissolving freely into the activating solution. Therefore, it is likely that either the free Sr^{2+} or NO_3^- ions are reacting with the ions in solution, preventing the complete dissolution of the aluminosilicate precursor or preventing the reaction of the aluminate and silicate monomers to form the fully reacted geopolymer matrix.

Fig. 3(c) shows that the introduction of the $\text{Sr}(\text{NO}_3)_2$ salt in all of the samples leads to a lower total cumulative heat when compared to the KGP control sample. The decrease in cumulative heat increases with the Sr/Al ratio, suggesting that the total extent of reaction is directly affected by the introduction of the salt. The heat release after 144 hours corresponds to roughly two thirds of the total heat release of the system for PC, and if this is assumed to be the same for geopolymer systems, the maximum total heat release for the $\text{Sr}(\text{NO}_3)_2$ containing geopolymer samples will be around 315 J g^{-1} maximum, with the NO_3_5 sample having the lowest total heat release of $\sim 250 \text{ J g}^{-1}$.²⁵ For all samples, the cumulative heat released 24 h after reaction is below the guideline value of 180 J g^{-1} (at 24 h) set by the current UK requirements for cement encapsulants for radioactive waste.^{26,27} Fig. 3 shows that the total heat release of the reaction can be decreased with the addition of certain salts, in this case $\text{Sr}(\text{NO}_3)_2$. If the integrity of the final product is found to be unaffected, this can be used to engineer the wasteform in order to meet the standards set within the UK.

3.3.2 Zeta potential measurements. Fig. 4 shows that metakaolin in the KOH solution without the presence of salts, shown by a Sr/Al ratio of 0, has a very negative surface charge. Upon the addition of the $\text{Sr}(\text{NO}_3)_2$, the zeta potential of the metakaolin particles at both pH 10 and 12 increases significantly to at or around 0 mV, the isoelectric point. At this point, the surface charge of the metakaolin is net neutral due to the effect of the electric double layer (EDL), promoting agglomeration over time.^{32,33} At low Sr/Al ratios, those of 0.025 and 0.05, the increase in pH from pH 10 to pH 12 reduces the change in recorded zeta potential, however, as the Sr/Al ratio increases to 0.075 and beyond, the effect is comparable at both pH points. The solubility of the $\text{Sr}(\text{NO}_3)_2$ is very high, and is unaffected by the high pH of the systems here. It also suggests that at pH 14, the nominal pH at which many of the samples used in other areas of this work reside, the $\text{Sr}(\text{NO}_3)_2$ will dissolve and have a similar effect. Therefore, the concentration of Sr^{2+} cations within the solution is very high, leading to significant changes to the zeta potential and causing the net charge around the surface of the metakaolin to be effectively 0, at the isoelectric point.

Similar to the mechanisms discussed above for samples produced with $\text{Sr}(\text{OH})_2 \cdot 8\text{H}_2\text{O}$, there are two mechanisms responsible for this. The net neutral charge results in a lack of electrostatic repulsion between the metakaolin particles, which will reduce dispersion and lead to the formation of larger metakaolin particle agglomerates with a decreased surface area available to participate in reaction during dissolution, and therefore a reduction in the rate of dissolution of metakaolin.^{29,30} Additionally, the formation of a layer of Sr^{2+} ions on the surface of the metakaolin particles produces a physicochemical barrier that simultaneously lowers the concentration gradient between the metakaolin and the surrounding solution and shields the surface of the aluminosilicate solid from OH^- ions in solution, which as a consequence are prevented from breaking the interlayer and intralayer bonds in metakaolin and preventing dissolution.³¹ This is supported by the high concentration of Sr^{2+} particles that are in solution due to the high solubility of the $\text{Sr}(\text{NO}_3)_2$. This mechanism is likely to be the cause for the impact on the reaction kinetics that can be seen in the ICC for these samples (Fig. 1c). As the Sr/Al ratio increases, the high solubility of the salt results in the concentration of Sr^{2+} cations within the solution to increase which, in turn, promotes the agglomeration of the metakaolin particles through interaction with the negative surface which leads to the slower dissolution of the metakaolin and a decrease in the reaction speed overall.

3.3.3 X-ray diffraction. The XRD data for geopolymers incorporating $\text{Sr}(\text{NO}_3)_2$ show a broad feature due to diffuse scattering, consistent the formation of the K-A-S-H gel, and also exhibit diffraction peaks due to the presence of niter (KNO_3 , PDF # 01-071-1558) suggests that the NO_3^- ions in solution due to the dissolution of the $\text{Sr}(\text{NO}_3)_2$ are reacting with the aqueous K^+ ions to precipitate out a solid crystalline K phase. This phase becomes more prominent with increasing Sr/Al ratio, with the greatest concentration in the NO_3_3 and



NO₃–5 samples and very little evidence of it in the NO₃–1 sample. This aligns with a greater concentration of NO₃[–] ions in solution. The increase in the concentration of this phase also contributes to the delay seen in the ICC, as the increase in Sr/Al ratio leads to a greater interaction with the K in the activating solution. This will slow the reaction to form the geopolymer and explains the difference in the ICC curves between the samples of differing Sr/Al ratios.

The presence of strontianite (SrCO₃, PDF #00-005-0418) is most likely due to the carbonation of the sample due to contact with the air, and the amount of this phase appears to increase with increasing Sr/Al. The presence of anatase (TiO₂, PDF # 01-084-1286) arises due to its inert nature and presence as an impurity in the metakaolin used in this study.

3.4 Geopolymers incorporating SrSO₄

3.4.1 Isothermal conduction calorimetry. The addition of the SrSO₄ in all of the samples has a noticeable impact on the kinetics of the reaction, in some cases even doubling the time taken for the maximum heat evolution to occur when compared to the control geopolymer sample as seen in Fig. 1(d). For the SO₄–5 sample, the value of this maximum heat evolved decreases by ~45% when compared to the KGP control. The difference in maximum heat flow between the SO₄–1, SO₄–2 and SO₄–3 samples is minimal, with the main difference being the time at which this maximum heat occurs increasing with increasing Sr/Al ratio. The time period between the initial dissolution of metakaolin (the peak that is not visible in Fig. 1d) and the observed reaction peak increases with increasing Sr/Al ratio.

Fig. 3(d) visualises the effect of increasing the Sr/Al ratio on both the maximum observed heat evolution and the corresponding time of this maximum. As is seen in Fig. 1(d), increasing the Sr/Al ratio leads to a decrease in the value of the maximum heat flow observed, as well as an increase in the time it takes for this to occur after the initial reaction. The SrSO₄ salt dissolves readily in the activating solution, releasing the Sr²⁺ cation and the SO₄^{2–} anion into solution. This means it is unlikely that the SrSO₄ is acting as a filler material and reducing the heat evolution in this manner. It is possible that the ions released during the dissolution of the salt reacts or interacts with either the metakaolin or the activating solution, which disrupts the dissolution of the metakaolin required to release the aluminate and silicate species needed to drive formation of the alkali aluminosilicate gel. This trend is shown in Fig. 3(d), although the cumulative heat for the SO₄–3 sample is noticeably higher than would be expected.

3.4.2 Zeta potential measurements. Fig. 4 shows that at pH 10, the introduction of SrSO₄ leads to a significant increase in the recorded zeta potential at all of the Sr/Al ratios. However, there does not appear to be a noticeable difference between the change seen at an Sr/Al ratio of 0.025 when compared with an Sr/Al ratio of 0.050, 0.075, 0.100, and 0.125. This suggests that, at pH 10, the SrSO₄ is saturated within the solution at an Sr/Al ratio of 0.025.

At pH 12, the effect on the zeta potential caused by the SrSO₄ is far less significant, suggesting the presence of a lower concentration of Sr²⁺ cations in these dispersions. Moreover, in contrast to observations for these dispersions at pH 10, the increase in the Sr/Al ratio at intervals of 0.025 leads to a continued increase in the zeta potential. These results indicate that the solubility of the SrSO₄ decreases with increasing pH, and therefore that it is unlikely that the adsorption of the Sr²⁺ cations to the surface of the metakaolin particles is the main mechanism for the retardation of the reaction seen in the ICC (Fig. 1d). As the pH increases (*i.e.* up to pH 14), the solubility of the SrSO₄ is likely to decrease further, resulting in a lower concentration of Sr²⁺ cations within the solution which will lead to a lower magnitude change in the surface charge of the metakaolin. Therefore, this mechanism will not lead to the significant changes seen in the ICC and suggests that it may arise due to SrSO₄ reacting with the activating solution, which then lowers the pH of the fresh state geopolymer reaction mixture, and retards reaction.

3.4.3 X-ray diffraction. The XRD data for geopolymers incorporating SrSO₄ show a broad feature due to diffuse scattering, consistent the formation of the K-A-S-H gel, and also exhibit diffraction peaks due the presence of celestine (SrSO₄, PDF # 04-009-9879), confirming that not all of the SrSO₄ dissolves into the activating solution. The presence of this becomes greater with increasing Sr/Al ratio, suggesting that the solubility limit is reached between the SO₄–1 and SO₄–2 samples. This would explain the zeta potential results (Fig. 4), where the increase in zeta potential decreases as the Sr/Al ratio increases. The presence of arcanite (K₂SO₄, PDF #00-024-0703) suggests that the dissolved SO₄^{2–} anions react with the K⁺ ions in solution to precipitate a solid, crystalline K₂SO₄ phase. The presence of this also increases with increasing Sr/Al ratio, suggesting that, as more SrSO₄ dissolves, there are more SO₄^{2–} anions available to react with the K⁺ cations as would be expected. This is similar for the kalistrontite (K₂Sr(SO₄)₂, PDF # 04-025-4251), which increases in prominence as mass of SrSO₄ in the sample increases. The formation of kalistrontite is not unexpected, as it is seen in the literature that deposits of kalistrontite have been found in the presence of SrSO₄ and K-bearing phases.^{35,36} The presence of this crystalline solid could explain the changes seen to the reaction kinetics in the ICC (Fig. 1(d)), as the SrSO₄ clearly reacts with the activating solution upon its addition. The crystallisation, and probable resultant precipitation, of this solid will prevent the migration of the activating solution fully around the solid metakaolin. Moreover, the consumption of both K⁺ and Sr²⁺, the two cations within solution that are responsible for the charge balancing of the AlO₄[–] sites in the gel phase, could result in less of the K-A-S-H gel being able to form in a stable state. For a combination of these reasons, the heat of reaction is less than that of the control KGP geopolymer when SrSO₄ is added to the mix. The presence of strontianite (SrCO₃, PDF # 00-005-0418) is most likely due to the carbonation of the sample *via* contact with air. The presence of anatase (TiO₂, PDF # 01-086-1157) arises due to its inert nature and presence as an impurity in the metakaolin used in this study.



Table 3 A summary of the effects of the Sr salts on the reaction kinetics of the geopolymer and the mechanisms responsible

Salt	Retards the reaction?	Reduces maximum heat flow?	Mechanism
Sr(OH) ₂ ·8H ₂ O	✓	✓	Filler effect + adsorbs to the surface of the metakaolin
SrCO ₃	X	✓	Filler effect
Sr(NO ₃) ₂	✓	✓	Adsorbs to the surface of the metakaolin + reaction with the activating solution
SrSO ₄	✓	✓	Filler effect + reaction with the activating solution + adsorbs to the surface of the metakaolin

4. Implications of this work

The findings presented here suggest that the Sr salts that are being termed as waste can actually prolong the reaction to form the geopolymer in the early stages of reaction. This is potentially industrially advantageous; as not only does this allow the 'waste' to act as a key constituent in the reaction process, it reduces the need for further chemical admixtures to achieve this, reducing the costs and technical complexity of the process, in addition to negating the need for incorporation of a potential organic complexant into the wasteform. The inclusion of some of the Sr salts also significantly lowers the heat of reaction observed for the geopolymers, which is important when considering scale up of this technology to an industrial process, as well as allowing the geopolymer systems to contain further elements that may be ideal for inclusion in this waste form, but are more sensitive to higher temperatures.

Future investigations focusing on the impact of the inclusion of Sr(OH)₂·8H₂O, SrCO₃, Sr(NO₃)₂, SrSO₄ and other Sr containing compounds into the geopolymer mix over a longer time scale, as well as the effect of the order of component addition, will allow for a more complete understanding of the materials performance. Research into the long term physicochemical properties of the material, long term phase evolution and leaching tests are necessary to build a complete understanding of the suitability of geopolymers for the disposal of Sr-containing radioactive waste.

5. Conclusions

This work investigated the impact of incorporating various salts of non-radioactive isotopes of strontium (Sr) on the kinetics and mechanisms of the reaction within the fresh geopolymer cement paste, and early stage K-A-S-H gel formation of potassium silicate-activated geopolymers. The chemical environments created by the introduction of Sr(OH)₂·8H₂O, SrCO₃, Sr(NO₃)₂ and SrSO₄ to the geopolymer reaction mixture simulate the potential interactions observed during geopolymer cementation of complex waste streams.

The introduction of the Sr salts into the geopolymer reaction mixture in all cases leads to a reduction in the heat evolved during the reaction to form the K-A-S-H gel in the first 6 days. From these findings, the mechanisms responsible for this change can be described separately: (a) the filler effect does not affect the time of maximum heat evolution, only reducing the value of the maximum heat flow, (b) the Sr²⁺

adsorbing to the surface of the metakaolin both reduces the value of the maximum heat flow and retards the reaction in a relationship where these extents are greater as the solubility of the Sr salt increases, (c) the reaction of the Sr salt with the activating solution leads mainly to a reduction in the maximum recorded heat flow, however, this may also be responsible for some retardation of the reaction. The mechanisms for the alteration of the reaction kinetics discussed here caused by the different Sr salts are shown in Table 3.

The findings of this work show that the incorporation of waste containing Sr salts can affect the kinetics of formation of a metakaolin-based, potassium silicate-activated geopolymer, however in all cases the formation of the K-A-S-H gel is observed. This suggests that these systems show great promise as wasteforms for the immobilisation of radioactive waste streams containing ⁹⁰Sr.

Conflicts of interest

There are no conflicts to declare.

Data availability

All data supporting this article have been included as part of the main manuscript.

Acknowledgements

This work has been funded by the Engineering and Physical Sciences Research Council (EPSRC), UK, through grant EP/Y029208/1, and a PhD Studentship funded by The University of Sheffield. We acknowledge and thank Professor John L. Provis and Dr Mark Ogden for insightful discussions during the early stages of this work.

References

- 1 A. I. Marsh, L. G. Williams and J. A. Lawrence, The important role and performance of engineered barriers in a UK geological disposal facility for higher activity radioactive waste, *Prog. Nucl. Energy*, 2021, **137**, 103736.
- 2 G. Bar-Nes, *et al.*, Cesium and Strontium Immobilization in Portland Cement Pastes Blended With Pozzolanic Additives, *J. Nucl. Eng. Radiat. Sci.*, 2017, **3**(3), 030907.



- 3 M. I. Ojovan, W. E. Lee and S. N. Kalmykov, *An introduction to nuclear waste immobilisation*, Elsevier, 2019.
- 4 L. Dezerald, *et al.*, Cement as a waste form for nuclear fission products: the case of ^{90}Sr and its daughters, *Environ. Sci. Technol.*, 2015, **49**(22), 13676–13683.
- 5 J. Tits, *et al.*, Strontium binding by calcium silicate hydrates, *J. Colloid Interface Sci.*, 2006, **300**(1), 78–87.
- 6 Radioactive Waste Management, *Geological disposal: waste package evolution status report*, RWM-NDA, Didcot, UK, 2016.
- 7 J. Lehne and F. Preston, *Making concrete change: Innovation in low-carbon cement and concrete*, 2018.
- 8 Nuclear Decommissioning Authority, Radioactive Waste Management, and Sellafield Limited, *Case study - Forward planning to ensure cement supplies*. 2019.
- 9 B. Walkley and J. L. Provis, Solid-state nuclear magnetic resonance spectroscopy of cements, *Mater. Today Adv.*, 2019, **1**, 100007.
- 10 A. C. Yildirim, K. Toda and T. Saito, Determination of the sorption mechanisms of sodium-alkalinized metakaolin-based geopolymers, *Appl. Clay Sci.*, 2024, **251**, 107303.
- 11 X. Niu, *et al.*, Adsorption behaviour of simulant radionuclide cations and anions in metakaolin-based geopolymer, *J. Hazard. Mater.*, 2022, **429**, 128373.
- 12 D. A. Geddes, *et al.*, Alkali-mediated Sr incorporation mechanism and binding capacity of alkali aluminosilicate hydrate in geopolymers, *J. Hazard. Mater.*, 2025, **488**, 137426.
- 13 X. Niu, *et al.*, Incorporation of boron into metakaolin-based geopolymers for radionuclide immobilisation and neutron capture potential, *Cem. Concr. Res.*, 2025, **190**, 107814.
- 14 J. L. Provis and S. A. Bernal, Geopolymers and related alkali-activated materials, *Annu. Rev. Mater. Res.*, 2014, **44**, 299–327.
- 15 J. L. Provis, G. C. Lukey and J. S. van Deventer, Do geopolymers actually contain nanocrystalline zeolites? A reexamination of existing results, *Chem. Mater.*, 2005, **17**(12), 3075–3085.
- 16 D. Geddes, *et al.*, *Metakaolin-based geopolymers for nuclear waste encapsulation*, in *Calcined Clays for Sustainable Concrete: Proceedings of the 2nd International Conference on Calcined Clays for Sustainable Concrete*, Springer, 2018.
- 17 J. d. Gasperi, *et al.*, Effect of Activator Type and Concentration, Water-to-Solid Ratio, and Time on the Flowability of Metakaolin-Based Geopolymer Pastes, *J. Mater. Civ. Eng.*, 2022, **34**(9), 04022205.
- 18 K. Vance, *et al.*, Observations on the rheological response of alkali activated fly ash suspensions: the role of activator type and concentration, *Rheol. Acta*, 2014, **53**, 843–855.
- 19 P. D. Silva, K. Sagoe-Crenstil and V. Sirivivatnanon, Kinetics of geopolymerization: Role of Al_2O_3 and SiO_2 , *Cem. Concr. Res.*, 2007, **37**(4), 512–518.
- 20 J. L. Provis and C. A. Rees, 7 - Geopolymer synthesis kinetics, in *Geopolymers*, ed. J. L. Provis and J. S. J. van Deventer, Woodhead Publishing, 2009, pp. 118–136.
- 21 T. Hofelich, *et al.*, The Isothermal Heat Conduction Calorimeter: A Versatile Instrument for Studying Processes in Physics, Chemistry, and Biology, *J. Chem. Educ.*, 2001, **78**, 1080.
- 22 B. Walkley, *et al.*, Incorporation of strontium and calcium in geopolymer gels, *J. Hazard. Mater.*, 2020, **382**, 121015.
- 23 X. Yao, *et al.*, Geopolymerization process of alkali–metakaolinite characterized by isothermal calorimetry, *Thermochim. Acta*, 2009, **493**(1–2), 49–54.
- 24 H. Reuter, S. Kamaha and O. Zerzouf, Hydrogen bonds in the crystal structure of strontium hydroxide octahydrate $\text{Sr}(\text{OH})_2 \cdot 8\text{H}_2\text{O}$, *Z. Naturforsch., B: J. Chem. Sci.*, 2007, **62**(2), 215–219.
- 25 F. Glasser and M. Atkins, Cements in Radioactive Waste Disposal, *MRS Bull.*, 1994, **19**(12), 33–38.
- 26 C. R. Wilding, The performance of cement based systems, *Cem. Concr. Res.*, 1992, **22**(2), 299–310.
- 27 M. Isaacs, *et al.*, Processing and product characteristics of a blended cement grout incorporating polycarboxylate ether superplasticiser, *Adv. Cem. Res.*, 2018, **30**(4), 148–158.
- 28 M. H. Derkani, *et al.*, Mechanisms of dispersion of metakaolin particles via adsorption of sodium naphthalene sulfonate formaldehyde polymer, *J. Colloid Interface Sci.*, 2022, **628**, 745–757.
- 29 H. Li, *et al.*, Salt coagulation or flocculation? In situ zeta potential study on ion correlation and slime coating with the presence of clay: A case of coal slurry aggregation, *Environ. Res.*, 2020, **189**, 109875.
- 30 A. H. Korayem, *et al.*, A review of dispersion of nanoparticles in cementitious matrices: Nanoparticle geometry perspective, *Constr. Build. Mater.*, 2017, **153**, 346–357.
- 31 P. Frugier, *et al.*, SON68 nuclear glass dissolution kinetics: Current state of knowledge and basis of the new GRAAL model, *J. Nucl. Mater.*, 2008, **380**(1), 8–21.
- 32 A. Kashani, *et al.*, The interrelationship between surface chemistry and rheology in alkali activated slag paste, *Constr. Build. Mater.*, 2014, **65**, 583–591.
- 33 S. Bhattacharjee, DLS and zeta potential – What they are and what they are not?, *J. Controlled Release*, 2016, **235**, 337–351.
- 34 P. Duxson, G. C. Lukey and J. S. J. van Deventer, Evolution of Gel Structure during Thermal Processing of Na-Geopolymer Gels, *Langmuir*, 2006, **22**(21), 8750–8757.
- 35 S. J. Kemp, *et al.*, Kalistrontite, its occurrence, structure, genesis, and significance for the evolution of potash deposits in North Yorkshire, UK, *Am. Mineral.*, 2018, **103**(7), 1136–1150.
- 36 S. Kemp, *et al.*, An improved approach to characterize potash-bearing evaporite deposits, evidenced in North Yorkshire, United Kingdom, *Econ. Geol.*, 2016, **111**(3), 719–742.

